UNIVERSITY UTRECHT

Utilization of scattered surface waves to image lateral discontinuities around Japan

by

Xiuying Chen

Supervisors: Elmer Ruigrok and Hanneke Paulssen

A thesis submitted in partial fulfillment for the
degree of Master of Science

in the
Faculty of Geosciences
Department of Earth Sciences

February 2017

UNIVERSITY UTRECHT

Abstract

Faculty of Geosciences
Department of Earth Sciences

Master of Science

by Xiuying Chen

Japan has both a dense coverage of seismic instruments and a rich distribution of large earthquakes. Its islands have been covered completely by Hi-net. Core-reflected phases are detected all over Japan, which are overlain by scattered surface waves. By applying muting and wavenumber filtering to isolate the scattered surface waves, potential scatterer areas become visible in south Japanese arc system. By applying Kirchhoff migration method, the imaging of a more focused scatterer model is obtained on the south edge of Okinawa Island. Previous studies of Okinawa region show positive contrast in velocity, magnetic and gravity anomalies in between the Keram Gap and Okinawa Island. The outcome of calculated reflection coefficient shows such agreement with the positive contrast. The formation of the scatterer might be due to three different extension fields: the extension of the backarc in northeast Okinawa Trough because of the horizontal mantel flow, the arc parallel extension all over the Trough except for the northwest part, and the arc perpendicular extension in southeast Ryukyu Arc area.

Key words: Scattered surface waves, imaging, Kirchhoff Migration, formation of Okinawa Trough

Acknowledgements

I would like to thank my family and my friends who are always supporting me during my student life overseas in Netherlands. And also I would like to thank Elmer for his flawless help and Hanneke for her helpful advice and suggestions for my thesis. I feel touched not only by their profound knowledge but also their dedicated attitude towards their career, which give me such inspiration and encouragement to learn and grow as much as I could in the future.

Contents

List of Figures

Chapter 1

Introduction

Surface-wave analysis is a key tool for seismology, ranging from near-surface characterization in geotechnical application to global seismology. Even though sometimes the surface waves are regarded as a kind of noise, the fact that the seismic records of scattered surface waves can be used to obtain images of certain earth structures is promising.

1.1 Tectonic setting overview of Japanese arc system

The Japanese islands lie at the junction of five tectonic plates in the western Pacific: the Pacific and the Philippine Sea oceanic plates, and Okhotsk, Eurasian and Amurian continental plates. Stretching south to the Kuril Islands and on to Japan, Kamchatka Peninsula sits at the junction of a triple plate collision between Okhotsk, North America and Pacific plates (Fig.1.1(a)). The tectonic situation is complicated in the area of Japanese arc system and Kamchatka Peninsula, where the North American, Okhotsk, Eurasian, Amurian and Philippine Sea Plate converge.

The Pacific Plate moves towards the northwest and is subducted beneath the Kuril Arc and the Izu - Bonin Arc (Wei et al., 1998). In the north, subduction of the Pacific Plate is oblique to the Kuril Trench. In addition to subduction of the Pacific plate underneath northeastern (NE) Honshu, the plate tectonic model show that east-west directed convergence between NE Japan (Okhotsk plate) and the Amur plate has initiated an incipient subduction zone on the eastern margin of the Japan Sea (Asahiko, 2001).

The Philippine Sea Plate moves towards the north and is subducting beneath south-western Japan and the Ryukyu Arc. In the south, the Philippine Sea Plate is also subducting obliquely to the Nankai Trough. The Ryukyu Arc is backed to the west within the Eurasian-Amurian Plate by a zone of active extensional rifting - the enlarging Okinawa Trough. This horizontal extensional field extends to the west of Kyushu.

There is also subduction of the Pacific Plate under the North American Plate and under Okhotsk Plate and constructed a line of active volcanoes stretching from central Kamchatka south to Japan.

1.2 Data

In the nineties of the 20th century, a large number of strong-motion, high-sensitivity, and broadband seismographs were installed to construct dense and uniform networks covering whole of Japan. This new broadband seismograph network consisting of 696 stations is called Hi-net, which is one of such receiver arrays that covers the complete island arc with approximately a 20 by 20 km sensor spacing (Okada et al., 2004). In this thesis, data that is processed is acquired by Hi-net detectors from NIED (National Research Instituted for Earth Science and Disaster Resilience). In total 666 out of 696 stations contributed the seismic data (Fig.1.3).

Japan has not only a dense coverage of seismic instruments but also a rich distribution of large earthquakes, which provides possibilities to select ideal events for the research. In this thesis eight events are picked for the data processing. They all have large magnitude (M >6) and distributed NE close to Japan main islands(Fig.1.2).

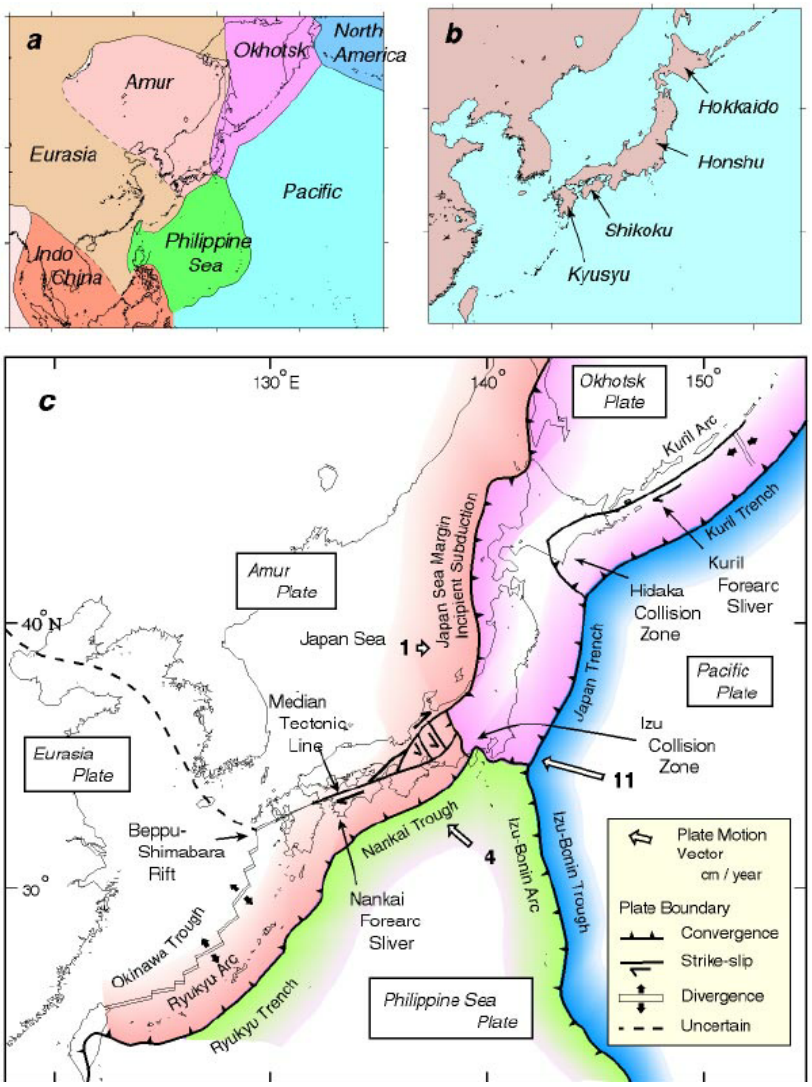

FIGURE 1.1: Plate tectonics of the Japanese arc system. (a) Plate tectonic framework of Northeastern Asia. (b) Distribution of four main islands of the Japanese arc system. (c) Plate boundaries of the Japanese arc system.(Source from Asahiko, 2001, Fig.1 from page 136)

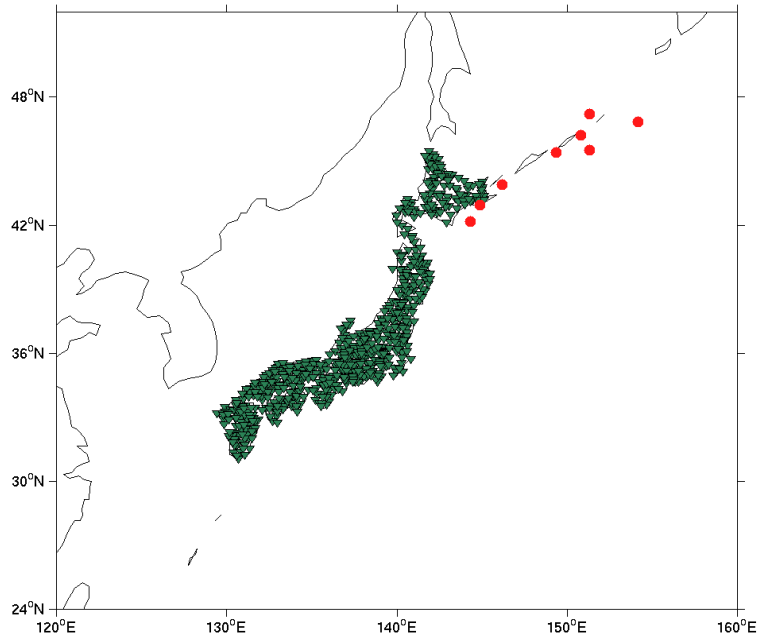

FIGURE 1.2: Distribution of Hi-net stations (green triangles) and earthquake events used in this thesis (red dots) in Japan

1.3 Problem Statement

For nearby and large-magnitude seismicity, Hi-net detects core-reflected phases all over Japan, such as ScS, PcP, ScP, etc. Part of these phases is overlain by phases with typical surface-wave velocities. Most likely, the latter phases are surface-wave reflections off lithospheric structure below Japan and surroundings.

In the outcomes of Fig.1.4, compared to the phases on radial component (R-component), one high move-out phase is only visible on transverse component. And most likely, it is an earthquake-related arrival. Another thing that could be observed from the phases on transverse component (T-component) is that, for two events at almost the same place, the steep move-out phases are almost identical. This is another indication that shows source-related and is not caused by microseism. Additionally, the phases get stronger when the magnitude of the earthquake is higher.

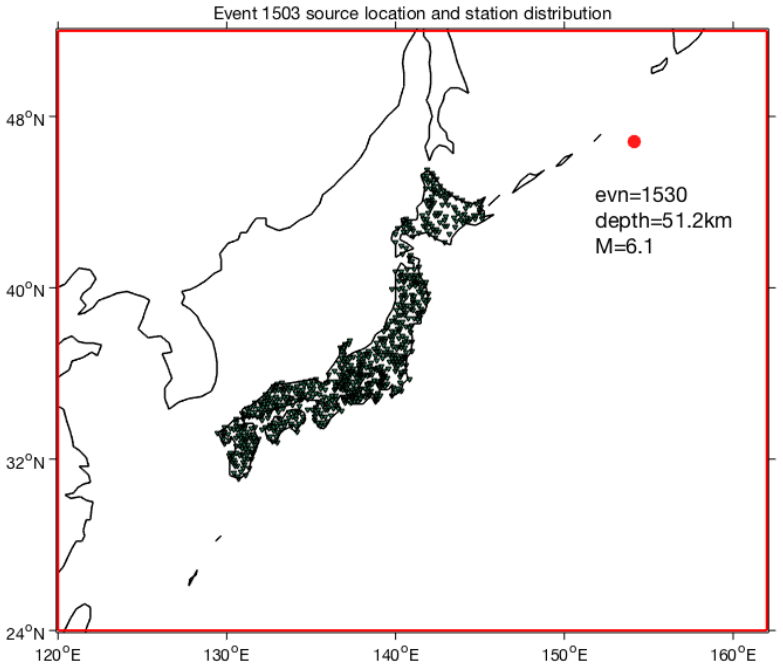

FIGURE 1.3: Distribution of the seismic stations(green triangles) and one of the earthquake events used in this thesis(red dot, signed as event 1503) in Japan. Event 1503 occurred in 15th October, 2005, of which the source depth was 51.2km and magnitude was 6.1

This research aims to confirm the nature of these phases and to use them for imaging potential lithospheric structure. Eight events will be processed in this thesis(Fig.1.5). In order to get visible imaging of potential scatterer areas, muting filter and wavenumber filter are going to be applied to isolate scattered surface waves(Chapter 2). By applying Kirchhoff migration method, the imaging of a more focused scatterer model will be obtained(Chapter 3). Combining with results of other relevant researches, interpretation of the scatterer and its formation will be made(Chapter 4).

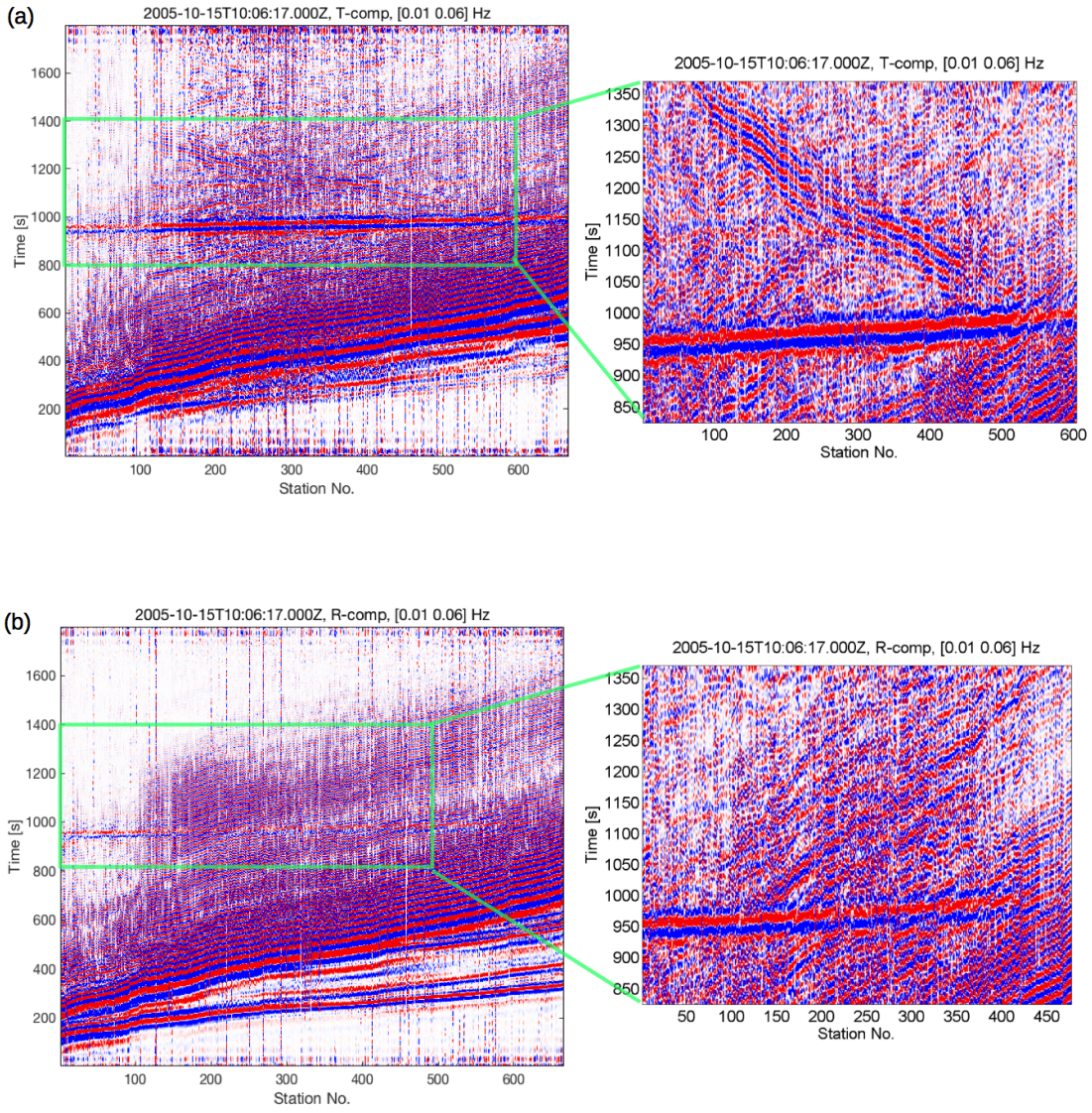

FIGURE 1.4: Phases of event 1503 on T-component and R-component from 0 to 1800 seconds after EOT (earthquake origin time). Filtered within frequency window $[0.01 - 0.06]$Hz. The source-receiver deistance increases with station numbers. In penal (a) the highlighted region is phases in time window $[800 - 1400]$s of first 600 stations. Clear high move-out phase is visible on T-component. In penal (b) the highlighted region is within time window $[0 - 500]$s of first 500 stations. No clear steep move-out phases is observed. In both penals (a) and (b), the large feature with small positive slope from 950 to 1000s is ScS, the S-wave reflected from core-mantle boundary(CMB).

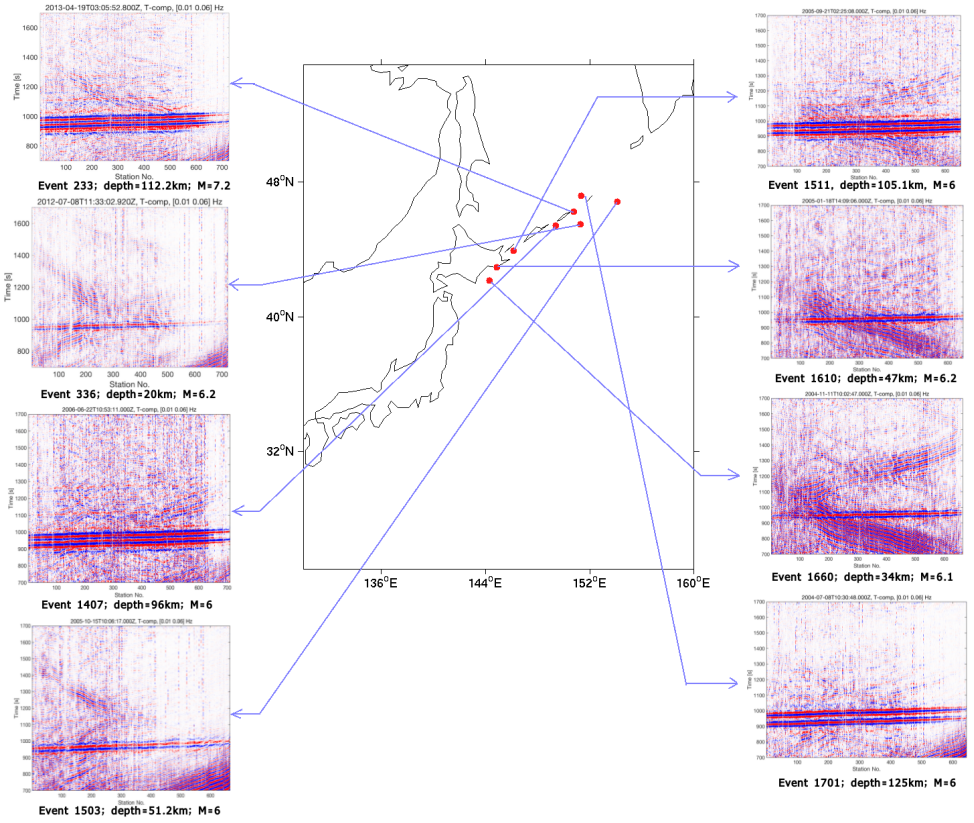

FIGURE 1.5: Source distribution of eight events used in this thesis, with the original wave phases. Event 1503 and 1660 have more visible scattered phases among the eight events. In the following these two events will be the examples to show the processing.

Chapter 2

Isolating scattered phases

Love waves travel in a side-to-side motion along the horizontal plane, while Rayleigh waves travel in the direction of propagation in the vertical plane. In Fig.1.4 shown in Chapter 1, the move-out phase is only visible on transverse component. Also, the apparent propagation velocity corresponds to that of a surface wave. Thus it is likely that this kind of phase is a Love wave. However, if the scattering was to occur from structure northwest or southeast of Japan, then it could be Rayleigh wave.

2.1 Frequency wavenumber filter

The time window shown in Fig.1.4(a) contains different types of phases: surface waves, surface wave scatterings, and body waves reflected by CMB. In order to obtain accurate images of potential scatterers, careful processing to separate the scattered components is required. Frequency wavenumber filter is tested in this research.

This signal processing is aimed to extract the scattered signals buried in all of the signals obtained. The frequency wavenumber (ω-k) filter is employed to modify the spectrum of the signals to frequency wavenumber (ω-k) domain.

The equation of frequency (ω) and wavenumber (k) is:

$$\frac{2\pi}{\lambda} = \frac{\omega}{v} = k$$

where λ is the wavelength, and v is the phase velocity of the wave.

The wavenumber filter is designed based on the Fourier transform. The input data is transformed from $t-x$ domain to ω-k domain. A linear event $f(t,x)$ in the $t-x$ domain can be described by a simple convolution equation:

$$f(t,x) = s(t) * \delta(t - tan(\alpha)x + b)$$

where $s(t)$ is a wavelet, α is the angle between the linear event and the space axis, b is the intercept of the event on the time axis.

The Fourier transformed expression is given as:

$$F(\omega,k) = S(\omega)e^{i\omega b}\delta(k - \omega tan(\alpha))$$

where, $S(\omega)$ is the Fourier transform of $s(t)$, linear event in the $t-x$ domain can be transformed into another linear event in the ω-k domain. The filter can help remove the unwanted signals from the input data. A rejection zone of a certain frequency window in the ω-k space will be defined to suppress and mute off waves that are not needed.

As shown in Fig.1.4(a), the scattered phases have the oblique slope downwards. Hence, the apparent velocity is negative. When spectrum is reformed into ω-k domain, the scattered phases have negative wavenumbers. In order to isolate the proposed phases, only the left side in Fig.2.1 was taken.

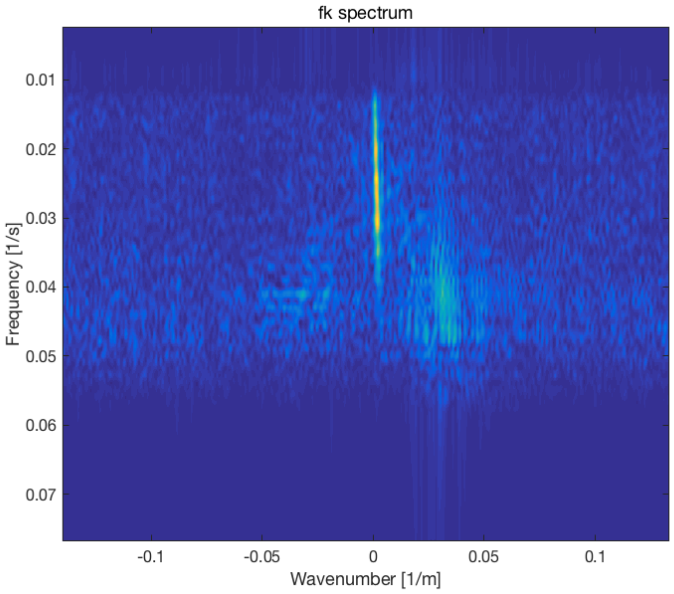

FIGURE 2.1: Original signals of event 1503 in ω-k domain within $[0.01 - 0.05]$ Hz. The highlighted feature near k=0 is ScS, the S-wave reflection from CMB. This feature needs to be suppressed, and spectrum in positive wavenumbers need to be rejected.

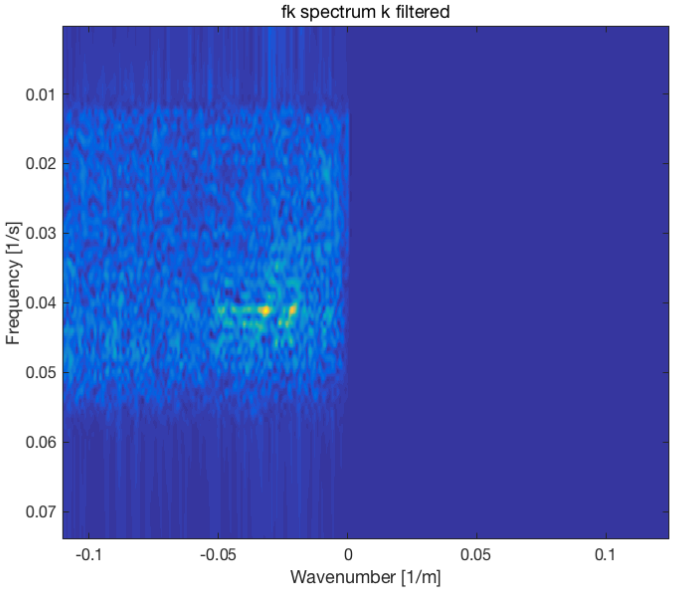

FIGURE 2.2: Filtered signals of event 1503 in ω-k domain within $[0.01 - 0.05]$ Hz after suppressing ScS and rejecting surface waves with positive wavenumbers.

The final frequency window is $[0.01 - 0.05]$Hz. Within the frequency band soft whitening is applied. The wavenumber filter is designed such that negative wavenumbers are passed and positive ones are rejected. The taper length is 10 in

samples. The above processing is done for time windows $[700 - 1800]$ s after earthquake origin time (EOT).

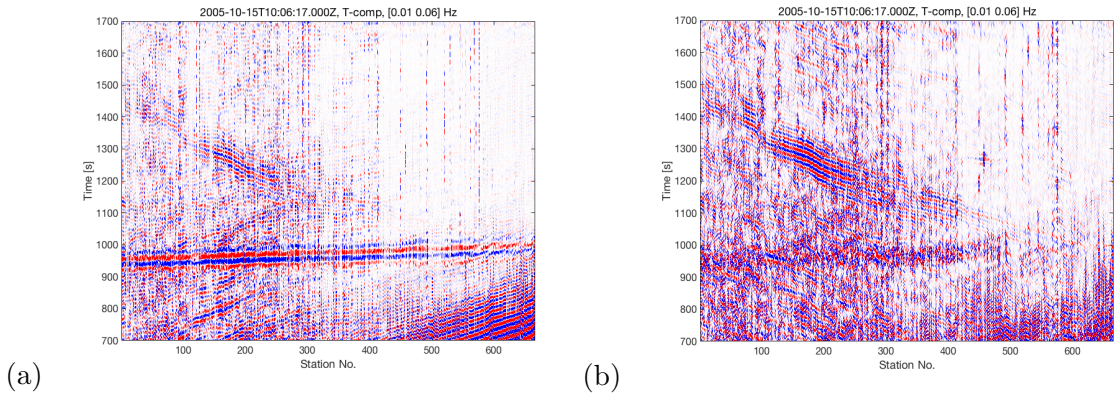

(a) (b)

FIGURE 2.3: Comparison between original data(a) and outcomes after applying ω-k filter (b). The scattered surface wave phases appeared strengthened after suppressing ScS.

2.2 Muting

In section 2.1 only the scattered energy, which has negative wavenumber value, is selected. However, the energy of ScS for certain events remains rather strong. Only by applying ω-k filter is not enough for acquiring a satisfied isolated scattered phase. In order to achieve a better filtering result, muting filter is applied before doing frequency wavenumber filtering. Steep-moveout phases that appear close to the arrival of ScS are isolated and saved(Fig.2.5). After moving off ScS, ω-k filter is applied to suppress phases with positive wavenumbers.

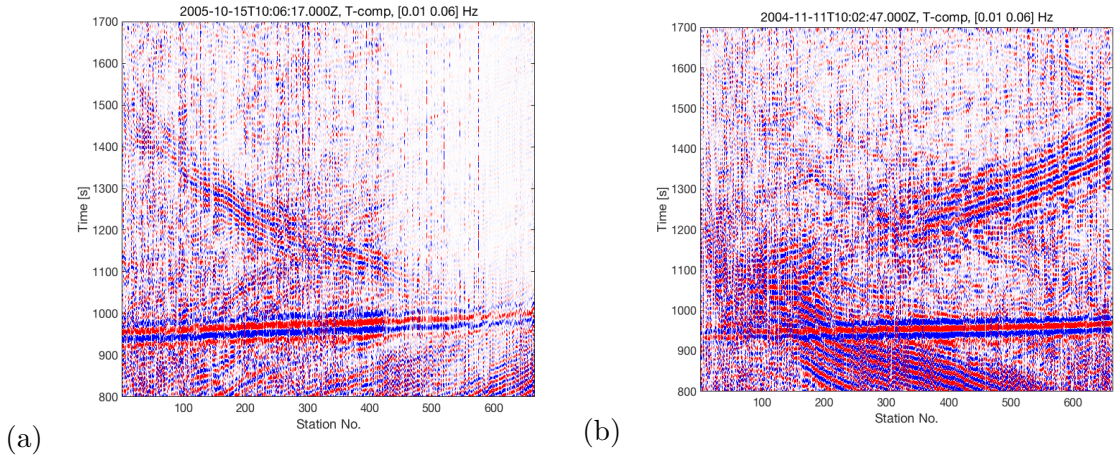

(a) (b)

FIGURE 2.4: Original wave phases of event 1503 (a) and 1660 (b)

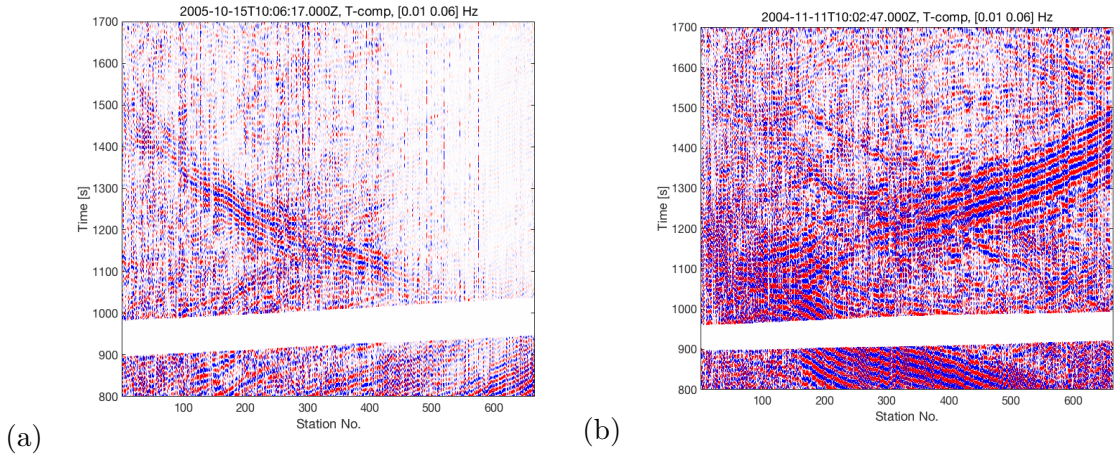

(a) (b)

FIGURE 2.5: Wave phases of event 1503 (a) and 1660 (b) after applying muting filter to move off ScS

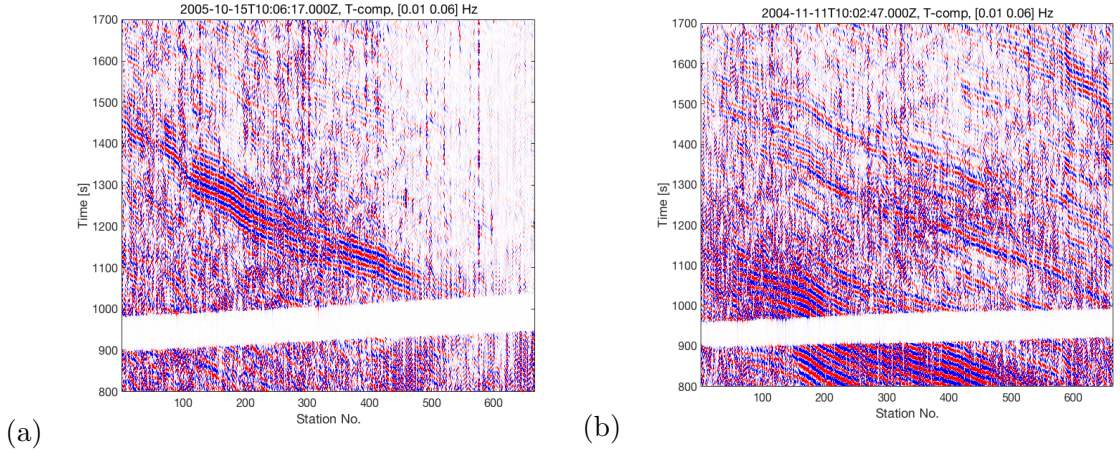

(a) (b)

FIGURE 2.6: Wave phases of event 1503 (a) and 1660 (b) after applying muting filter and ω-k filter. After moving off ScS, ω-k filter is applied to suppress phases with positive wavenumbers.

Chapter 3

Imaging scattered phases

As soon as the nature of these phases is confirmed, a sensible back projection can be set up to image the responsible structure. Such back projection will be tested using synthetic data. By identifying new phases, new structure below Japan and surroundings might be discovered.

3.1 Multiple scatterer approach - Kirchhoff migration

If a source and a geophone on the free surface, and a single reflector in a homogeneous medium are given, there will be only one primary reflection recorded in the seismic trace (Fig.3.1). The arrival time of this event is equal to the traveltime for energy to propagate from the source to the reflection point p and from p to the geophone. The dashed line in Fig.3.3 depicts the associated specular ray.

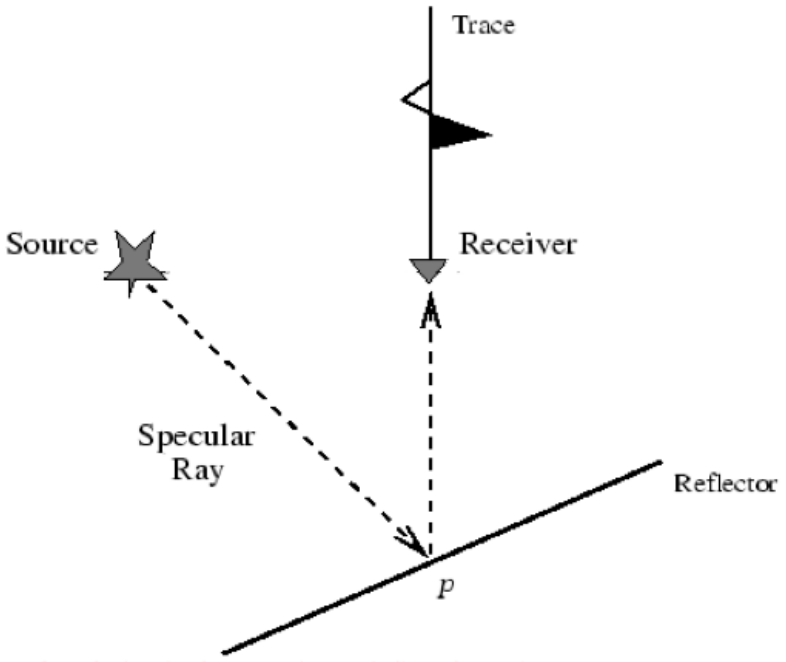

FIGURE 3.1: Seismic forward modeling for a homogeneous medium, where there is a single reflector. The only event being observed is a primary reflection (Source from Sun, 2001, Fig 2.1 from page 4)

If the locations and strengths of reflectors from data are given, the model will be computed through a process called 'migration' to get the imaging. This is the step is to apply Kirchhoff migration, which is to smear the observed energy to its primary reflection point. This is a blind operation because the true reflection point is unknown. The reflection needs to be migrated to all the possible image points r, whose reflection traveltime is equal to the observed traveltime of the reflection. Such as in Fig.3.2, the energy is smeared to points r_1, r_2 and r_3. The three points all satisfy the requirement of traveltime mentioned above. Furthermore, it is obvious that all of the possible image points can fill up as an entire ellipsoidal zone as shown in Fig.3.2.

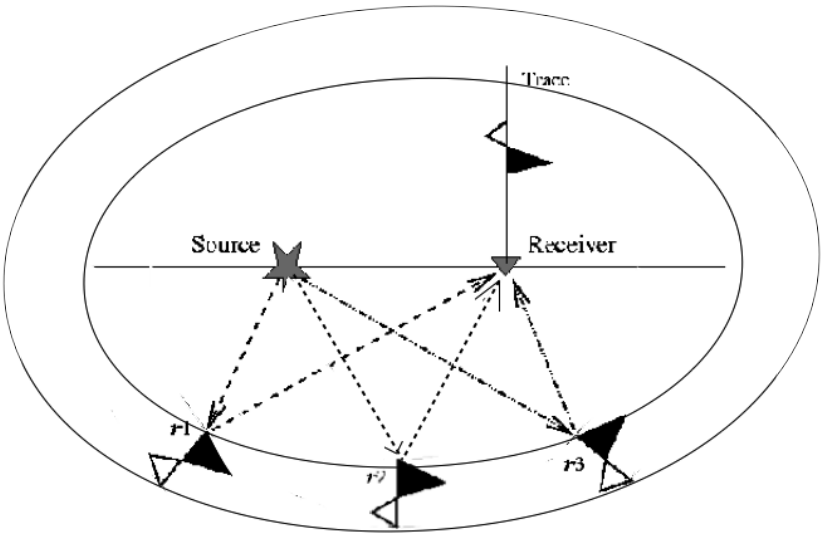

FIGURE 3.2: Full-aperture KM of a single trace. Each time sample on the trace is smeared along an ellipse, and each event is smeared along an ellipsoidal zone. (Modified from Sun, 2001, Fig.2.2 from page 5)

3.2 Potential subvertical scatters using primarily isolated scattered surface waves

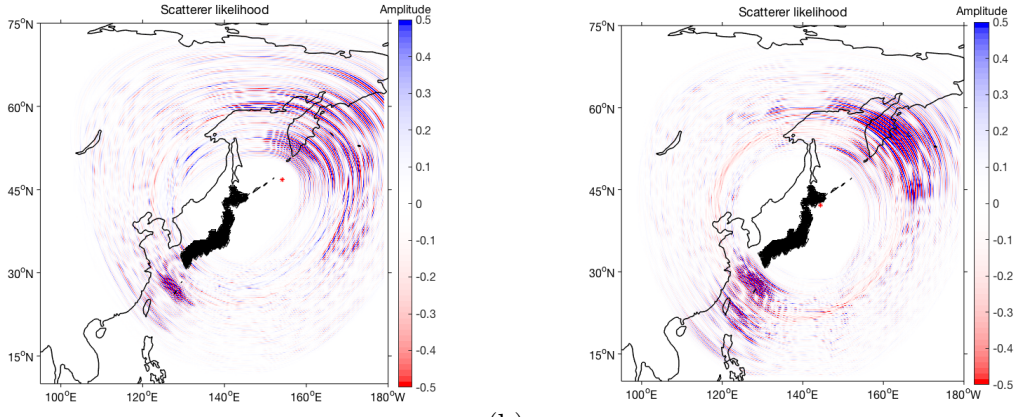

FIGURE 3.3: Outcomes of event 1503 (a) and 1660 (b) by only muting off ScS phases. There are two featured areas indicate highly potential scatterer structures in each panel. One is in the south part of Japanese arc system, the other is at Kamchatka Peninsula and its vicinity.

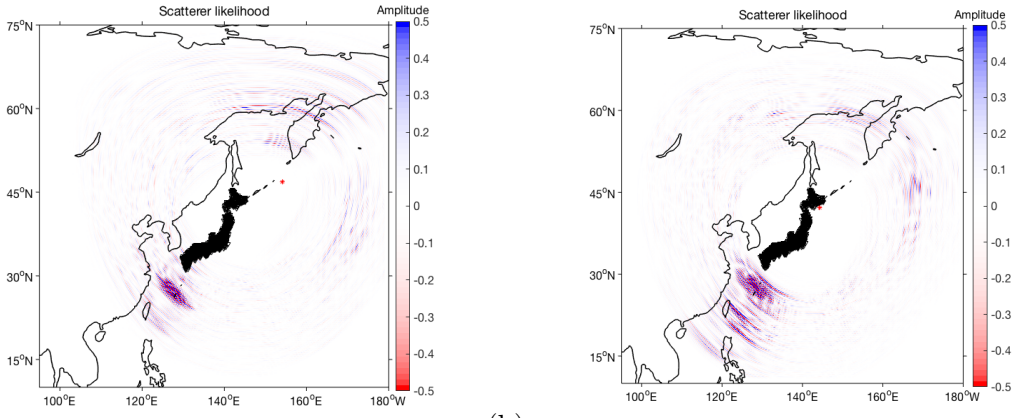

FIGURE 3.4: Outcomes of event 1503 (a) and 1660 (b) by muting off ScS phases and then applying ω-k filter. There is only one featured area in south part of Japanese arc system indicate highly potential scatterer structure in each panel.

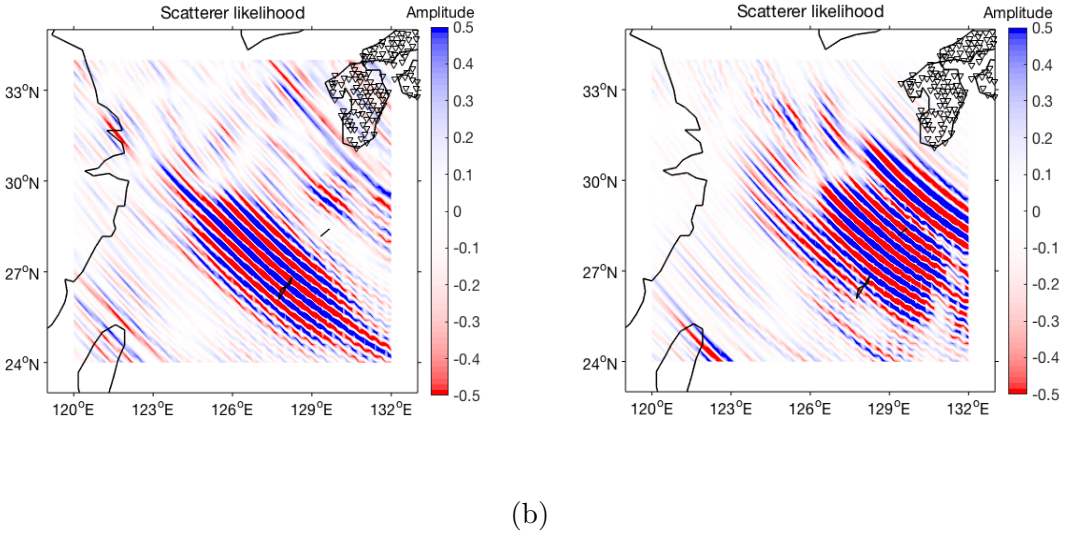

FIGURE 3.5: Outcomes of event 1503 (a) and 1660 (b) after applying muting and ω-k filter focusing on the featured area in Okinawa area in south part of Japanese arc system.

From the outcomes of scattering imaging, before applying ω-k filter, there are two major regions with highly potential scatterer. One region is in the south part of Japanese arc system, including Okinawa Trough and Okinawa Island, the other region is at Kamchatka Peninsula and its vicinity. After applying ω-k filter, there is only one featured area left in Okinawa. It indicates that the ω-k filter which suppressed phases with positive wavenumbers has suppressed scattering from northeast (Kamchatka area).

There is possibility that multiple scatterer structures could exist, but in this thesis we only focus on one primary potential scatterer.

3.3 Synthetic tests of imaging

Best imaging results are achieved when the reflectors have been illuminated from many different angles. However, despite the large amount of sources and receivers, the Japan configuration (Fig.1.1(b)) is limited in the sense that both sources and receivers are distributed primarily in a NE-SW line. Given this limited configuration, in the following we test how well potential reflectors could be imaged at different azimuths with respect to Japan. For this reason we use synthetic data. Best-fit velocity model is obtained by testing out different velocities to see if the scatterer point is on the isochron ellipse, and it is 3.95m/s. For the following processing, the primary potential scatterer model is set on the south edge of Okinawa Island according to the outcomes of eight events, including Fig.3.3. The location is $26.108°N$, $127.8°E$.

In the data processing, a standard source wavelet is generated by applying first derivative of Guassian with dominant frequency of 0.3Hz. Then forward Fourier transform is applied to the generated signal to do the forward modeling of response of the observed traveltime to reflection traveltime. The migration of reflection to all possible image points fill up as a highlighted isochron ellipse, where there is the potential scatterer structure locates.

Fig.3.6(a) shows the imaging result for one source-receiver configuration for one scatterers of an azimuth with respected to Japan. The scatterers are set in south of Okinawa Island, close to the boundary of Eurasia and Philippine Sea plates. The set scatterer is one point on the ellipse. When there is combination of multiple source-receiver configurations, the corresponding ellipses will intersect with each other, and the intersection area will become more intensive (Fig.3.6(b)). By combining the configurations of all receivers, the focused intersection will be the area of potential scatterer structure.

The synthetic outcomes (i.e. 'scatterer likelihood' in Fig.3.6, 3.7 and 3.8) for event 1503 and 1660 is shown in Fig.3.7. The scatterer model is just on the trace of the

migration ellipse. Fig.3.8 shows the final imaging outcome of the potential scatterer area after every of the eight events is smeared along an ellipsoidal zone and all the synthetic data is multiplied. The imaging area around the scatterer model is most highlighted in the south edge of Okinawa Island. The whole imaging is distributed in a NW-SE line from $27°N$, $126°E$ to $25°N$, $129°E$.

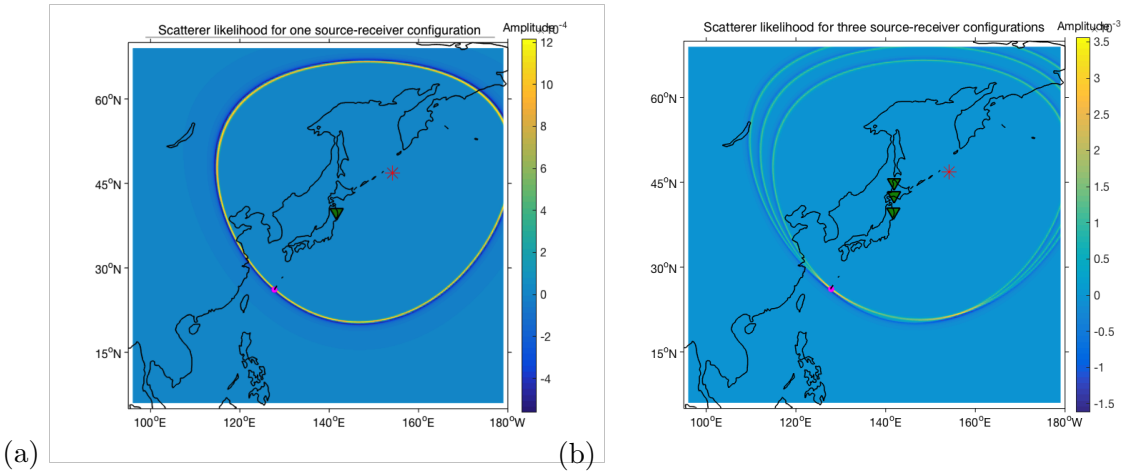

(a) (b)

FIGURE 3.6: Panel (a) shows the imaging result for one source-receiver configuration for one scatterers of an azimuth with respected to Japan. The scatterers are set in south of Okinawa Island. Panel (b) is the combination of three source-receiver configurations, the corresponding ellipses intersect with each other, and the intersection area will become more intensive.

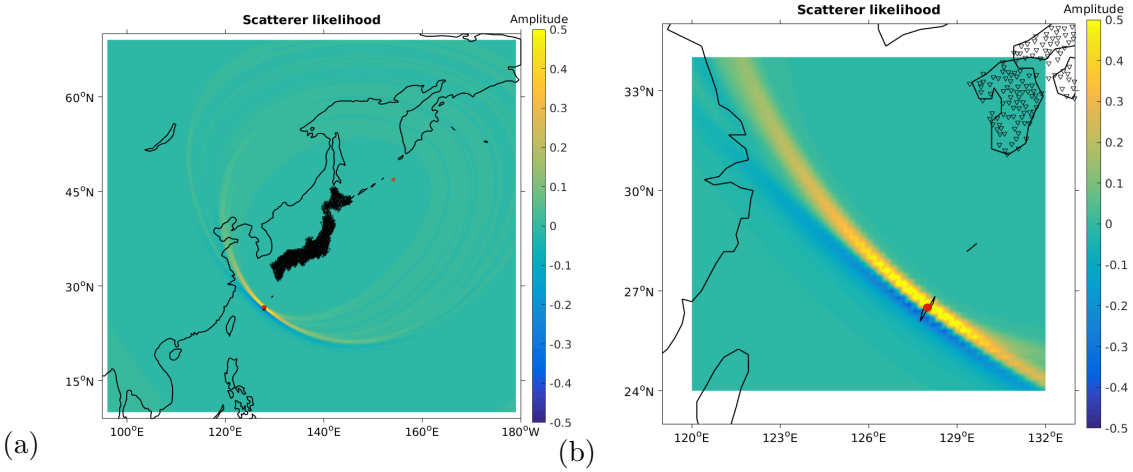

(a) (b)

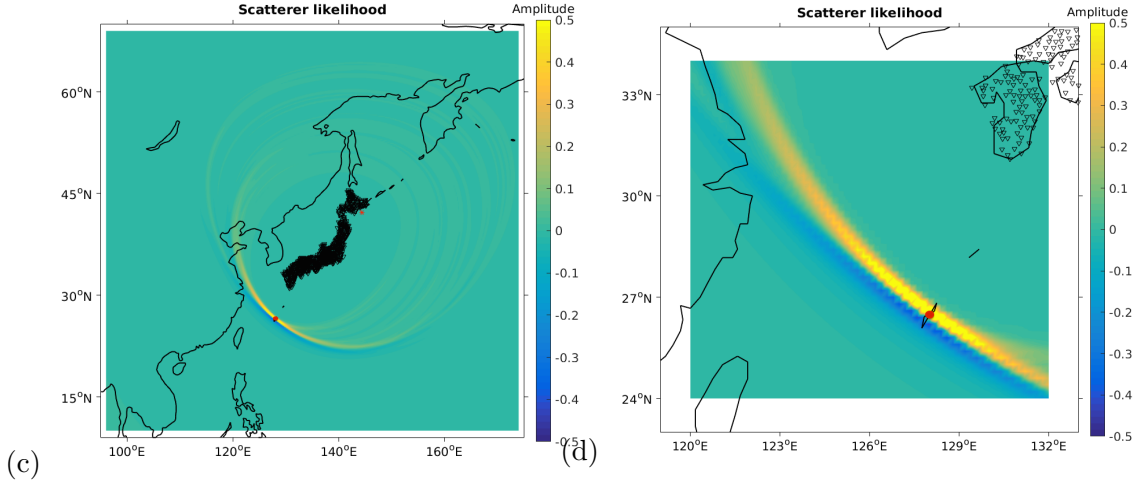

FIGURE 3.7: Synthetic data of potential scatterer location and areas for event 1503 ((a), (b)) and 1660 ((c), (d)). Panel (b) and (d) are zoomed focus on the highlighted potential scatterer areas

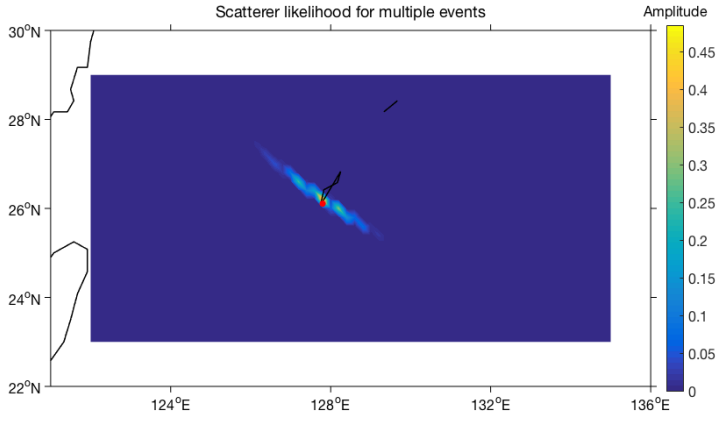

FIGURE 3.8: Final synthetic outcome of potential scatterer location and areas of all eight events. The red dot is the scatterer model applied in the processing.The area around the scatterer model is most highlighted in the south edge of Okinawa Island. The imaging area is distributed in a NW-SE line from $27°N$, $126°E$ to $25°N$, $129°E$.

3.3.1 Reflection coefficient

In order to find out more supporting evidence for the following interpretation, reflection coefficient is calculated. When diving into the reflection coefficient, linear fitting is applied to the isolated scattered surface waves and direct surface waves after filtering.

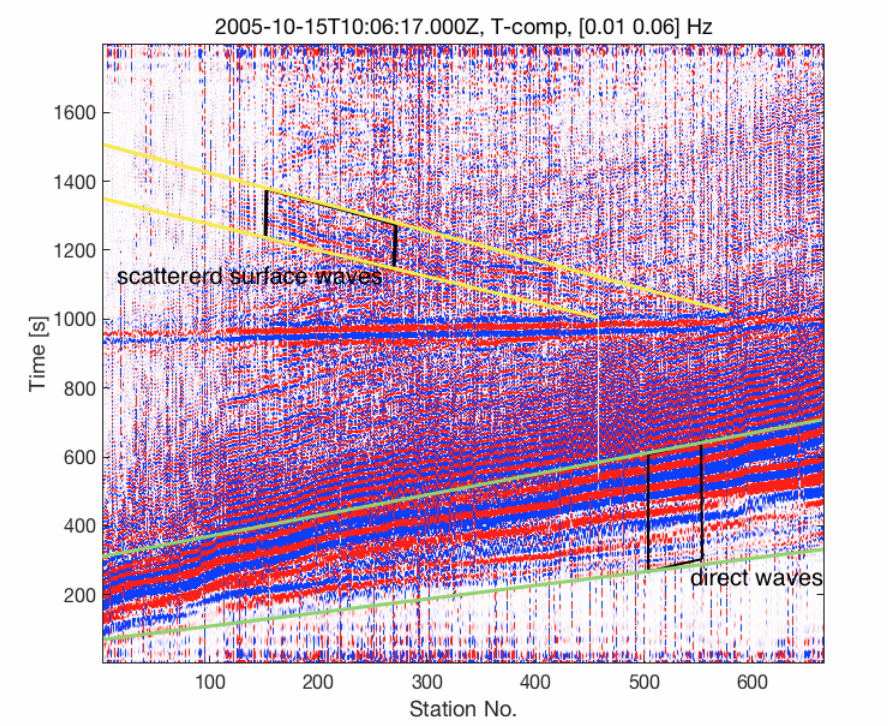

FIGURE 3.9: Original data without applying muting and wavenumber filtering of event 1503 within time window $[0-1800]$ seconds. The yellow highlighted phases are scattered surface waves, and the green highlighted phases are direct waves. Black framed phases are selected parts of the two kinds of phases that are separately isolated in calculating reflection coefficient.

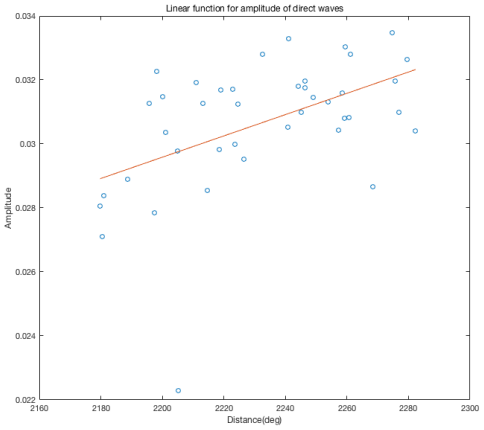

FIGURE 3.10: Linear fitting function for direct waves

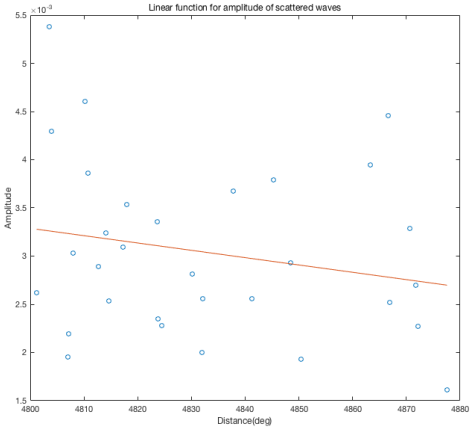

FIGURE 3.11: Linear fitting function for scattered waves

The distance between scatterer model and earthquake source of event 1503 is 32.65 in degree. According to the linear functions, when this distance is reached, the amplitudes of direct wave A_{DW}^{OK} and scattered wave A_{SC}^{OK} are 0.065 and 0.0149 respectively. The zero-offset reflection coefficient at Okinawa I^{OK} is defined as:

$$I^{OK} = A_{SC}^{OK} / A_{DW}^{OK}$$

Thus I^{OK} is equal to 0.229.

According to Aki's theory, the reflection coefficient can be defined as:

$$\grave{S}\acute{S} = \frac{\rho_1 v_1 A - \rho_2 v_2 B}{\rho_1 v_1 A + \rho_2 v_2 B}$$

where ρ_1 is the density of incident plane, ρ_2 is the density of refraction plane. v_1 and v_2 represent velocity of incident wave and refraction wave. A and B respectively denote cosine value of incident and refraction angle. According to the brief index figure of Fig.3.8 and the source-receiver configuration for the set scatterer model respect to Japan, the value of the incident and refraction angles are very tiny, so their cosine value A and B can be approximated to 1. Thus the reflection coefficient can be modified as:

$$I^{OK} = \frac{\rho_1 v_1 - \rho_2 v_2}{\rho_2 v_2 + \rho_1 v_1}$$

By the value of I^{OK} calculated out above, we can get: $v_1\rho_1$=0.63$v_2\rho_2$

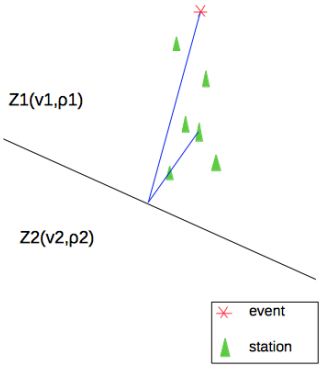

FIGURE 3.12: Brief index figure of $v_1\rho_1$ and $v_2\rho_2$

Chapter 4

Interpretation

4.1 Tectonic overview of Okinawa Trough and its vicinity in Ryukyu Arc System

The scatterer structure is located on the southeast of the middle part of Okinawa Trough. Okinawa Trough is a backarc basin located southeast of the Eurasian plate and northwest of the Ryukyu Trench (Wang et al., 2008). The Okinawa Trough is still rifting, and its opening is mainly caused by the Philippine Sea slab (PHS) subduction northwestward beneath the Eurasian plate from the Ryukyu Trench (Wang et al., 2008). Ryukyu Trench is part of the Ryukyu arc system, which extends from South Kyushu to North Taiwan, and includes the Ryukyu Arc and the Okinawa Trough as well (Fig.4.1). It has been indicated that the island arc system could be subdivided into the northern, central and southern Ryukyu Arc subsystems from northeast to southwest by the Tokara Strait (T.S.) and Keram Gap (K.G.).

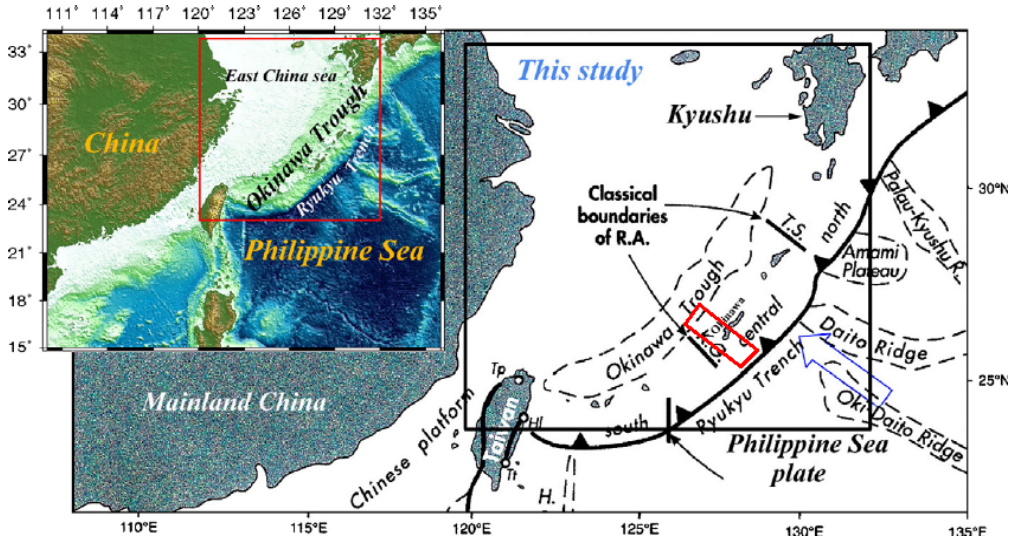

FIGURE 4.1: Topographic map and tectonics in the Ryukyu Arc system and its surrounding regions. A blue arrow shows that the Philippine Sea plate is subducting northwestward from the Ryukyu Trench. The red squared zone, between the southern part of Okinawa Island and K.G., is the region that will be discussed in this thesis. (Modified from source Wang et al., 2008, Fig.1 in page 2)

4.2 Velocity anomalies

It is clear that the high-velocity zone related to the PHS slab is not very continuous along the Ryukyu Arc system(Wang et al., 2008). The gradient images in Fig.4.2 at depths of 40-80 km show visible boundaries in the gradient variations at the location of K.G.. Also in this figure, there is positive contrast of velocity anomalies between the south part of Okinawa Island and south edge of K.G., which is within the area of the imaging outcomes in Chapter 2 and 3. The reflection coefficient outcome at the end of Chapter 3 shows agreement with the positive contrast of velocity anomalies. However, Fig.4.2 presents the velocity variation of P wave. The velocity variation of Love wave (S_H) tends to be larger than V_P by the effect of potential fluid structure on S_H waves. The previous studies suggested that the Ryukyu Arc system could be subdivided into three sub-blocks by the sub-boundaries, showing general agreement with the patterns of the velocity perturbations from the tomographic results along the arc system.

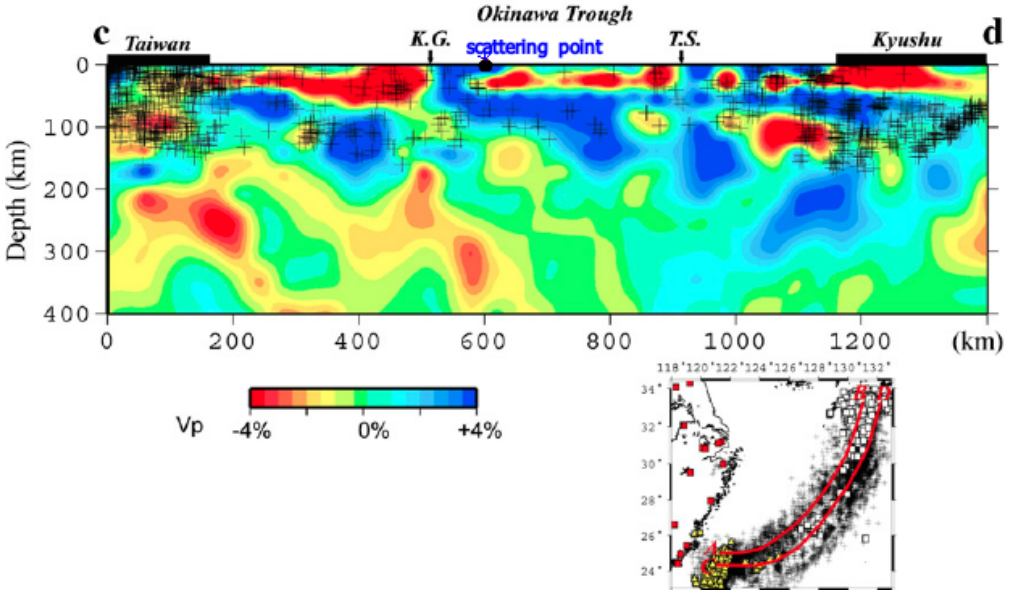

FIGURE 4.2: Vertical sections along the lines parallel to the Ryukyu Trench shown in the insert map. Blue color and red color show high-velocity anomaly and low-velocity anomaly respectively. Scattering point has been marked in blue triangle.(Modified from Wang et al., 2008, Fig.11 from page 9)

4.3 Magnetic anomalies

Fig.4.3 comes from the magnetic anomalies compiled by the CCOP (Coordinating Committee for Geoscience Programmes in the East and Southeast Asia), and the corresponding data set gives a general overview of the equivalent magnetization distribution (Hsu et al., 2001). The inversion results show that the belts in the Ryukyu subduction system are parallel to the Ryukyu trench. It implies that rifting of the middle and northern Okinawa Trough was initiated along the eastern side of the Taiwan-Sinzi belt and has been mainly controlled by the oblique subduction of the Philippine Sea plate beneath the Ryukyu arc. The southern Okinawa Trough, rifted since early Pleistocene, is distinct from the middle and northern Okinawa Trough by a high-magnetization zone (Hsu et al.,2001). According to the magnetic inversion by Hsu et al., the potential scatterer region exhibits low magnetization while the northeast and southwest of its edges is expressed by relatively high magnetization.

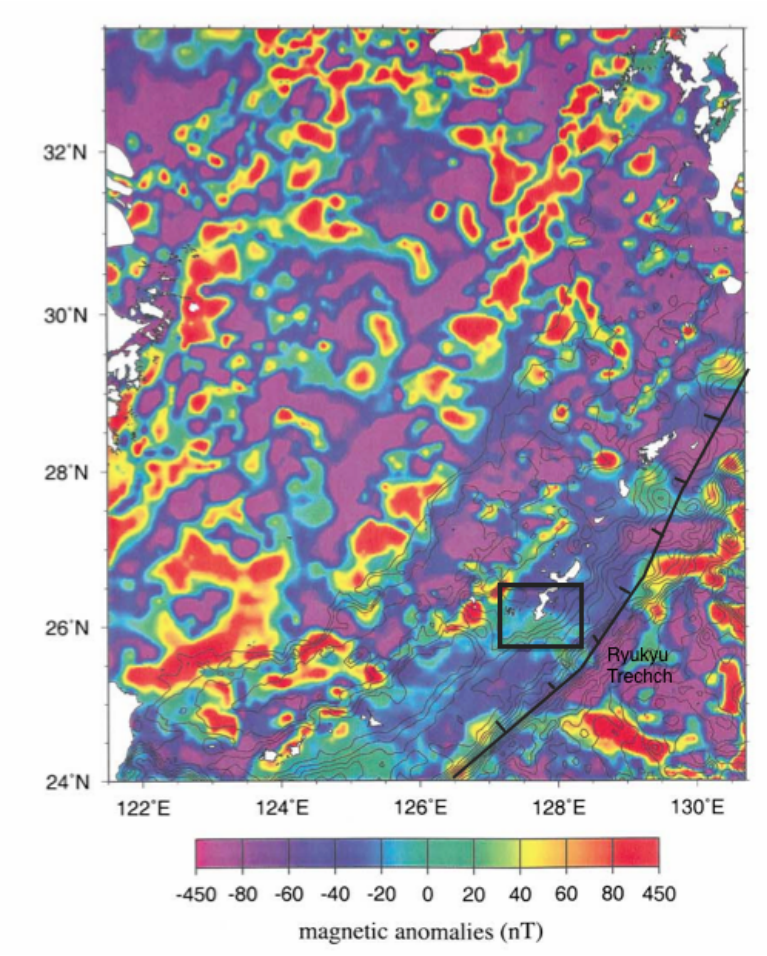

FIGURE 4.3: Magnetic anomalies. Same area scale as Fig.3.3 and Fig.3.6. Black line highlighted area is where the potential scatterer structure locates. (Modified from Hsu et al.,2001, Fig.4(a) from page 6)

4.4 Gravity anomalies

Gravity maps also exhibit strong variations at the locations of the sub-boundary in K.G., which coincide with the perturbations of the velocity images at depths of 20-120 km and the patterns of the gradient images in Fig.4.2. In Fig.4.4 the squared area, the gravity is relatively lower in the potential scatterer region than its north side, Okinawa Island, and its south vicinity of K.G.. These features together with the velocity and magnetic images, may reflect the presence of the scatterer due to different convergence and evolution processes of the subducted PHS plate along the Ryuku Arc.

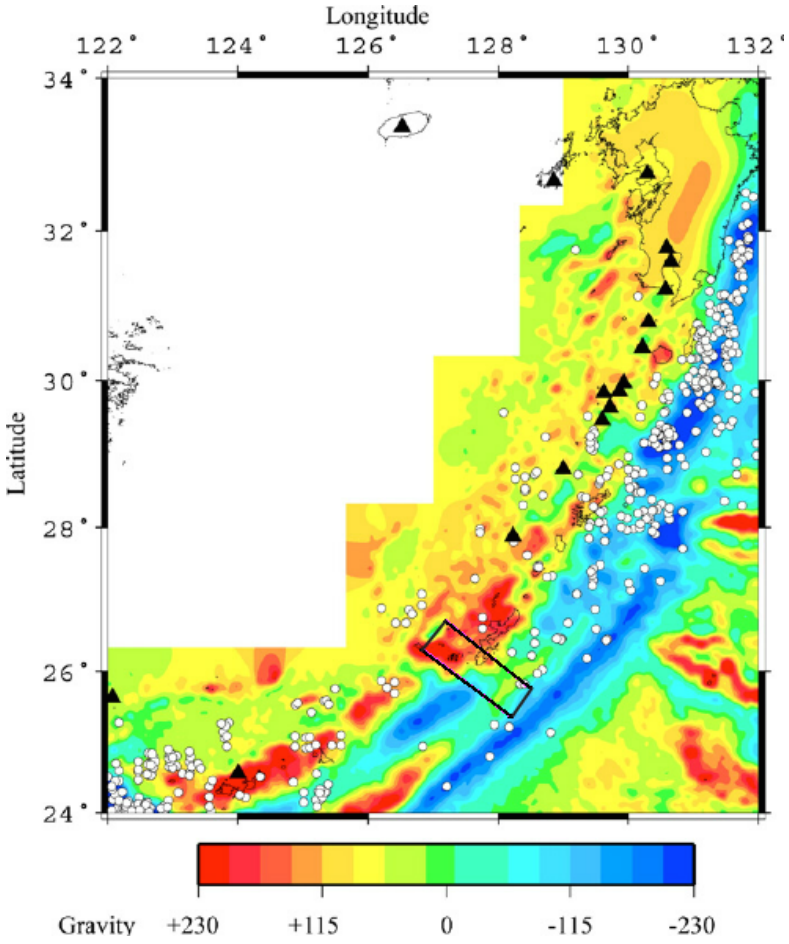

FIGURE 4.4: Gravity map. Same area scale as Fig.3.3 and Fig.3.6. Black line highlighted area is where the potential scatterer structure locates. (Modified from Wang et al., 2008, Fig.14 from page 12)

4.5 Summary

A large number of previous studies have discussed continental backarc rifting of the Okinawa Trough. Park et al. (1998) proposed a three-stage model of the trough opening based on analysis of the seismic reflection surveys. Along the Okinawa Trough, an arc-perpendicular extensional stress field is observed in the southeastern and central Ryukyu Arc, whilst in the northeastern Okinawa Trough, the direction of the extensional axis is oblique to both the arc normal direction and the direction of plate motion (Fabbri and Fournier, 1999; Kubo and Fukuyama, 2003). At the same time, an arc-parallel extensional stress field along the forearc was observed in the entire region of the Ryukyu Arc except in the northeastern area. This stress field is clearly separated from the backarc extensional stress field in the Okinawa Trough by

the volcanic chain (Fabbri and Fournier, 1999; Fournier et al., 2001; Kubo and Fukuyama, 2003). The differences revealed by velocity anomalies, together with the magnetic inversion and gravity images, may reflect the presence of individual sub-blocks of the Ryukyu Arc system due to different convergence and evolution process of the subducted PHS plate along the arc. The rifting of the middle and northern Okinawa Trough was initiated along the eastern side of the Taiwan-Sinzi belt. The Miocene extension for the middle and northern Okinawa Trough may be related to the opening of the Japan Sea and associated with a major strike-slip fault along the east side of Taiwan-Sinzi belt, which is mainly controlled by the oblique subduction of Philippine Sea plate beneath Ryukyu Arc. While the formation of southern Okinawa Trough is different from Middle and Northern Okinawa Trough. The rifting of Southern Okinawa Trough is in early Pleistocene, and is distinct from north and middle parts marked by high-gravity and high-magnetic anomalies. The formation of Okinawa Trough is very complex, including a multiple opening stages, which might be the cause of the potential existence of scatterer in between the K.G. and Okinawa Island. In conclusion, the scatterer might be formed due to three different extension fields: the extension of the backarc in northeast Okinawa Trough because of the horizontal mantel flow, the arc parallel extension all over the Trough except for the northwest part, and the arc perpendicular extension in southeast Ryukyu Arc area.

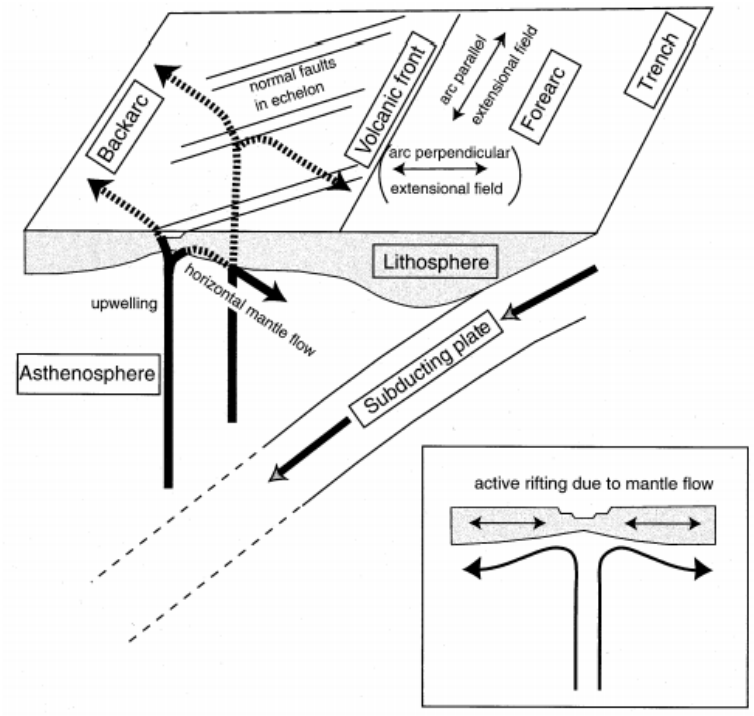

FIGURE 4.5: Possible mechanism(Kubo et al, 2002) schematic illustration of oblique relation between backarc stress structure and forearc stress structure. A possible mechanical interaction at the bottom of the lithosphere in the backarc is illustrated as a cause of oblique extension to the arc trend. A typical active rifting setting in two dimensions is shown in the lower right part for reference.

4.6 Discussion

In the data processing section, the quality of the dataset is not very satisfied because of the noise signals. Also there is limited quantity of seismic stations merely installed in Japan. Even though the seismographs are covered all the islands, they can not cover all the reflected surface waves from structure Okinawa regions. As for the interpretation, since the tectonic setting of Okinawa region is quite complex, in contrast of less abundant studies focusing on middle part of Okinawa Trough, it is difficult to give a more specific interpretation and final conclusion.

Chapter 5

Conclusion

By applying muting filter and wavenumber filter, scattered surface waves overlying the core-reflected phases below Japan and its surroundings are isolated to first locate the potential scatterer area, which is located in Okinawa region in south Japanese arc system . Best-fit velocity model is obtained by testing out different velocity to see if the set scatterer point is on the migration isochron ellipse. By applying Kirchhoff migration method with tested velocity model, the imaging of a more focused scatterer model is obtained on the south edge of Okinawa Island. Previous studies of Okinawa Trough show the obvious velocity, magnetic and gravity anomalies in between the Keram Gap and Okinawa Island, where show agreement with the outcome of calculated reflection coefficient, and is in coincidence with the imaging outcomes. The scatterer structure might be formed due to three different extension fields. However, since the complex formation of Okinawa Trough and complicated tectonic setting of Japanese arc system, and consider the possibility of multiple scatterer structures, a more convincing conclusion of the formation mechanism of imaged potential scatterer is still uncertain.

Chapter 6

Reference

[1] Aki K, Richards P G. Quantitative seismology[M]. 2002.

[2] Fabbri O, Fournier M. Extension in the southern Ryukyu arc (Japan): Link with oblique subduction and back arc rifting[J]. *Tectonics*, 1999, 18(3): 486-497.

[3] Hilde T. W. C, Kimura M, Ling-Yun C, et al. Back arc extension in the Okinawa Trough[J]. *Journal of Geophysical Research*, 1987, 92(B13): 14,041-14,063.

[4] Hsu S K, Sibuet J C, Shyu C T. Magnetic inversion in the East China Sea and Okinawa Trough: tectonic implications[J]. *Tectonophysics*, 2001, 333(1): 111-122.

[5] Kubo A, Fukuyama E. Stress field along the Ryukyu Arc and the Okinawa Trough inferred from moment tensors of shallow earthquakes[J]. *Earth and Planetary Science Letters*, 2003, 210(1): 305-316.

[6] Lee C S, Shor G G, Bibee L D, et al. Okinawa Trough: origin of a back-arc basin[J]. *Marine Geology*, 1980, 35(1-3): 219-241.

[7] Okada Y, Kasahara K, Hori S, et al. Recent progress of seismic observation networks in Japan, Hi-net, F-net, K-NET and KiK-net[J]. *Earth, Planets and Space*, 2004, 56(8): xv-xxviii.

[8] Oshida A, Tamaki K, Kimura M. Origin of the magnetic anomalies in the southern Okinawa Trough[J]. *Journal of geomagnetism and geoelectricity*, 1992, 44(5): 345-359.

[9] Shiono K, Mikumo T, Ishikawa Y. Tectonics of the Kyushu-Ryukyu arc as evidenced from seismicity and focal mechanism of shallow to intermediate-depth earthquakes[J]. *Journal of Physics of the Earth*, 1980, 28(1): 17-43.

[10] Su W, Woodward R L, Dziewonski A M. Deep origin of mid-ocean-ridge seismic velocity anomalies[J]. *Nature*, 1992, 360(6400): 149-152.

[11] Taira A. Tectonic evolution of the Japanese island arc system[J]. *Annual Review of Earth and Planetary Sciences*, 2001, 29(1): 109-134.

[12] Wang Z, Huang R, Huang J, et al. P-wave velocity and gradient images beneath the Okinawa Trough[J]. *Tectonophysics*, 2008, 455(1): 1-13.

[13] Wei D, Seno T. Determination of the Amurian plate motion[J]. *Mantle dynamics and plate interactions in East Asia*, 1998: 337-346.

[14] Yilmaz, O. and S.M. Doherty, 1987. Seismic Data Processing (Investigations in Geophysics, Vol. 2). *Society of Exploration Geophysicists*, USA.

[15] Sun H. Wavepath migration for depth imaging and velocity analysis[D]. The University of Utah, 2001.